frontiers | Frontiers in Marine Science

ORIGINAL RESEARCH
published: 22 April 2022
doi: 10.3389/fmars.2022.848757

Impacts of Climate Change and Human Perturbations on Organic Carbon Burial in the Pearl River Estuary Over the Last Century

Wenpeng Li[1,2], Xinxin Li[1,2], Xin Zhao[1], Chengpeng Sun[1], Tianyi Nie[1], Yumei Hu[1] and Chunzai Wang[3]*

[1] Department of Ocean Science and Engineering, Southern University of Science and Technology, Shenzhen, China, [2] Southern Marine Science and Engineering Guangdong Laboratory (Guangzhou), Guangzhou, China, [3] State Key Laboratory of Tropical Oceanography, South China Sea Institute of Oceanology, Chinese Academy of Sciences, Guangzhou, China

Estuaries have experienced significant changes due to global climate change and human perturbations since the last century. However, the climate and anthropogenic influence on the burial of sedimentary organic carbon (OC) in estuaries is still not understood well yet. Here, a 3-meter sediment core was taken from the Pearl River Estuary (PRE) in China. Depth profiles of both bulk OC and lignin biomarker data indicated three stages with different features of buried OC during the 130-year sediment deposition. The 1893-1957 stage showed 20% more burial of marine derived OC, which was mostly adsorbed on finer minerals compared to the years after 1957. The 1957-1980 period witnessed 4.6 times higher burial rate of petrogenic OC, which made the radiocarbon age of total organic carbon 42% older than before due to soil erosion and carbonate rock weathering. The 7-year running average variation of terrestrial OC input based on endmember mixing model was correlated with the Pacific Decadal Oscillation index before 1957, but correlated with the Atlantic Multidecadal Oscillation between 1957 and 1980 in the region. The reduction of land derived OC content after 1980s was mostly affected by human perturbations such as deforestation and dam construction which corresponded to the beginning of Economic Reform and Open Up in China. The overall increase of lignin content from bottom to surface sediment indicated increased vascular plant derived OC due to deforestation activities during the urbanization process. The study suggested different time periods when climate or human disturbance dominantly affected the OC burial in the PRE, which have significant indications for local and global carbon cycling and environmental ecology.

Keywords: Pearl River Estuary, organic carbon, lignin, Atlantic Multidecadal Oscillation, deforestation, hydrodynamics

OPEN ACCESS

Edited by:
Zhaohui Zhang,
Zhejiang University, China

Reviewed by:
Rienk H. Smittenberg,
Stockholm University, Sweden
Rui Bao,
Ocean University of China, China
Karl Ljung,
Lund University, Sweden

***Correspondence:**
Xinxin Li
lixinxin@sustech.edu.cn

Specialty section:
This article was submitted to Marine Biogeochemistry, a section of the journal Frontiers in Marine Science

Received: *05 January 2022*
Accepted: *28 March 2022*
Published: *22 April 2022*

Citation:
Li W, Li X, Zhao X, Sun C, Nie T, Hu Y and Wang C (2022) Impacts of Climate Change and Human Perturbations on Organic Carbon Burial in the Pearl River Estuary Over the Last Century. Front. Mar. Sci. 9:848757. doi: 10.3389/fmars.2022.848757

1 INTRODUCTION

The estuaries are major components of the global carbon cycle (Canuel and Hardison, 2016). Estuaries are hotspots for organic carbon (OC) burial (Bianchi et al., 2018) that is a global benefit for warming (Breithaupt et al., 2020). However, the estuaries are also "carbon incinerators" (Aller and Blair, 2006) with high OC remineralization rates (Chen et al., 2022) which can be affected by local and global environmental changes, as well as human perturbations (Syvitski et al., 2022). Therefore, understanding changes in OC biogeochemistry during sediment burial in the estuaries is essential to better understand the role they play in global climate change (Bianchi and Allison, 2009).

Stratigraphic change of OC burial can result from the combined effect of climate change and human perturbations. Sediment records provide an alternative method to analyze the impact of extreme events on sediment deposition and OC burial in coastal estuaries (e.g. Wheatcroft et al., 2010; Swindles et al., 2018) over extended time periods. For example, the stable carbon isotopes and terrestrial biomarkers have been applied as efficient indicators (Dalzell et al., 2005; Clark et al., 2013; Li et al., 2013; Li et al., 2020) of transportation and deposition of flooding induced terrestrial OC in coastal sediment cores in China (Wu et al., 2007). The rainfall frequency in China has been reported to be affected by the Pacific Decadal Oscillation (PDO) (Qian and Zhou, 2014; Wu and Mao, 2017). The Atlantic Multidecadal Oscillation (AMO) may also control the extreme weather and climate events including monsoon occurrence, runoff, and rainfall in China (Li and Bates, 2007; Qian et al., 2014) which affected the delivery of sediment and terrestrial OC to estuaries. Moreover, human activities have increasingly affected soil erosion and the delivery of terrestrial OC (Wang et al., 2018; Ye et al., 2021) to estuaries in China. Therefore, the organic carbon burial in coastal sediment of China is controlled by multiple processes.

The Pearl River Estuary (PRE) acts significantly in the "source to sink" process of OC cycling by linking the Pearl River to the South China Sea. With a population of ~100 million, the region of the PRE has become one of the fastest developing regions in China over the past decades. The human activities such as dam constructions (Wu et al., 2016), deforestation (Liu et al., 2014) has influenced the PRE sedimentation (Owen and Lee, 2004; Ye et al., 2021), subaqueous topography, ecological environment (Wu et al., 2016; Wu et al., 2018), and potentially the delivery of OC to the of PRE. Meanwhile, the climate effect on the local and national precipitation and drought have been widely studied (Duan et al., 2013; Drinkwater et al., 2014; Yang et al., 2017b). However, the climate effect on the variation of sediment deposition and OC burial in the PRE has rarely been well studied on decadal to centennial scales. Considering climate change and human perturbation have become significant drivers that may translate to simultaneous responses in sediments records, delineating their influences on sediment and OC burial is becoming significant to understand the changes of OC cycling to more intensified extreme human and climate events in recent years.

This study aimed to address this knowledge gap using multiple proxies to identify how the OC burial in the sediment record responded to human perturbations and climate effects. Bulk carbon proxies including total organic carbon (TOC) and total nitrogen (TN), stable isotopes ($\delta^{13}C$), radiocarbon ($\Delta^{14}C$), and terrestrial organic biomarker of lignin were analyzed in a ^{210}Pb-dated core to examine the sources and composition changes of OC in the PRE over the last century. The variation of terrestrial OC input was then compared with the climate oscillation index, human activities, and sediment mineralogy to explore the mechanisms for OC burial during the sedimentation process in the PRE.

2 SAMPLING AND METHODS

2.1 Site Description and Sample Collection

Nearly half of the Pearl River water discharges into the SCS through the PRE *via* three main tributaries in the lower drainage basin: North River, West River, and East River (**Figure 1**). A 3-meter gravity core was collected at 21-m water depth off Guishan Island in the PRE (22.1315°N, 113.8055°E) in October 2017. The core was sectioned at an interval of 5cm for 0–100 cm and 10cm for 100–300 cm. The samples were immediately stored at -80°C until further analysis.

2.2 ^{210}Pb Chronology

The total ^{210}Pb ($^{210}Pb_t$), ^{226}Ra, and ^{137}Cs activities were analyzed in dry samples (6~9g) with a low background high-purity germanium (HPGe) γ-ray detector (EG& G Ortec Ltd., USA)

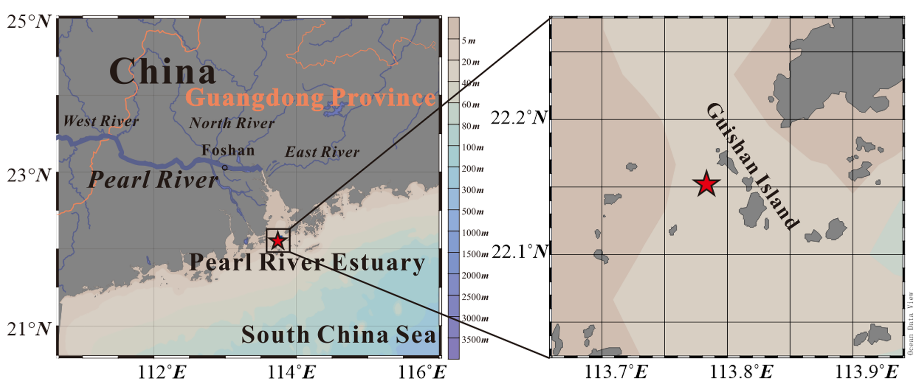

FIGURE 1 | Sampling site of the sediment core from Guishan Island, Pearl River Estuary. The three main tributaries of North River, West River, and East River are labeled.

at the State Key Laboratory of Marine Geology, Tongji University. The samples were sealed in polyethylene tubes to allow for radioactive equilibration for 30 days before analysis (Ye et al., 2020).

The activities of ^{137}Cs were too low to obtain any confident results, therefore only ^{210}Pb dating was used in this study. ^{226}Ra was used as an index of supported ^{210}Pb ($^{210}Pb_{su}$), and excess ^{210}Pb ($^{210}Pb_{ex}$) activities were calculated by subtracting $^{210}Pb_{su}$ activities from $^{210}Pb_t$ activities. The sediment accumulation rate (SAR) was then calculated with the constant rate of supply (CRS) model which assumes that the flux of ^{210}Pb to the accumulating sediment is constant during a timescale of 100–200 years. The chronology was derived by fitting the exponential ^{210}Pb decay profiles with the cumulative dry mass (Appleby and Oldfield, 1978; Zhang et al., 2014; Li et al., 2021). Fitting analysis was done using the 'Exp2PMod1' function in the Origin 2021 program.

2.3 Bulk Carbon/Nitrogen, Stable and Radiocarbon Isotope Analysis

Sediment samples are first floated in deionized water, dispersed through agitation, and then sieved to <180 microns to remove any root materials. Then the <180 microns organic sediment size fraction is treated with a series of hot (~ 70-90°C) acid leaches with HCl at a concentration of 0.1N for a period of 4-12 hours. Additional applications of HCl are provided until any carbonate presence has been completely removed. Samples are then rinsed to neutral with deionized water and dried at 100°C until dry. The sediments are then homogenized to insure an equal dispersion of the available carbon. A small aliquot is then tested with concentrated HCl to check for completion of carbonate removal. The sample was then measured either in whole or where applicable appropriately sub-sampled for combustion and analysis. The TOC (%), TN (%) content was determined on an elemental analyzer (Vaio EL Cube, Germany) after decarbonation. Stable isotopes of TOC ($\delta^{13}C$) were measured using an isotope ratio mass spectrometer (Thermo Science Delta Plus, USA) connected on-line to an elemental analyzer (Carlo Erba Instruments Flash 1112, USA). The C/N ratio was calculated as the atomic ratio of TOC and TN. The ^{14}C of these samples was measured by accelerator mass spectrometer (AMS) interfaced with an elemental analyzer at the Beta Analytic testing laboratory, USA. Radiocarbon data were expressed as $\Delta^{14}C$ values and fraction modern (Fm).

2.4 Grain Size and Porosity

The grain size of the sediments was analyzed by a laser grain-size analyzer (Mastersizer 3000, Malven Instruments Ltd., UK) following the methodology described by Jiang et al. (2016). Briefly, about 0.2 g of the samples were treated with 15ml 10% (v/v) hydrogen peroxide to remove the organic matter. Carbonates were then removed by gradual addition of 15 ml of 10% HCl. The sample residue was dispersed with 10 ml of 10% $(NaPO_3)_6$ on an ultrasonic vibrator for 10 min before instrumental analysis. The particle sizes less than 4 μm were defined as clay, 4-63 μm as silt, and > 63 μm as sand. To sort the grain-size distribution into valuable information on geological processes and palaeo-environmental changes, end-member analysis (EMA) was applied to estimate end-member variations according to the methods by Prins et al. (2000). In this study, we used a newly developed GUI software of AnalySize for processing and unmixing grain size data (Paterson and Heslop, 2015) to determine the grain-size distributions of the detrital fraction in our sediment core. Porosity of each sample was calculated from the water content (wet-dry weight) prior to and after freeze-drying.

2.5 Lignin-Phenols Analyses

Lignin analyses were performed using CuO oxidation method of Hedges and Ertel (1982), as modified by Bianchi et al. (2002). Homogenized sediments containing ca. 3 to 5 mg of organic carbon were transferred to stainless-steel reaction vials with 330 ± 4 mg CuO and 3 to 5 ml 2 N NaOH in glove box purged by nitrogen and then digested at 150°C for 3 h. Reaction products were neutralized and extracted with diethyl ether (peroxides removed), filtered through combusted glass-fiber filled with glass wool, dried under N_2, and converted to trimethylsilyl derivatives using bis-(trimethylsilyl)-trifluoroacetamide (BSTFA). Lignin-phenol derivatives were analyzed with an Agilent 7890-Gas Chromatograph/5977-Mass Spectrometric Detector (GC–MS).

Quantification of lignin-phenols was based on a mixed standard calibration curve containing known amounts of 12 lignin reaction products of interest as well as the internal standard ethyl vanillin. Eight lignin-phenol oxidation monomer products (LOPs): C (ferulic acid+cinnamic acid), V (vanillin+acetovanillone+vanillic acid) and S (syringealdehyde+ acetosyringone+syringic acid) were quantified and used as molecular indicators for source and diagenetic state of terrestrial vascular plant tissue (Hedges and Parker, 1976). Compound of 3,5-dihydroxybenzoic acid (3,5Bd) was also derived after cupric oxidation and quantified (Goñi and Hedges, 1995). The precision for the total lignin phenols was within ±10%, while that for individual compound ranged from ±5 to ±15% based on triplicate analysis.

Lambda-8 (Λ_8),which is defined as the total weight in milligrams of the sum of C, V, and S phenols, normalized to 100 mg of organic carbon (Hedges and Parker, 1976), is used as a biomarker for terrestrial vascular plants. The acid-to-aldehyde ratios of both V and S phenols: (Ad/Al)v, (Ad/Al)s, were used as indicators of lignin degradation state prior to burial (Hedges et al., 1988). The C/V (woody/non-woody) and S/V (gymnosperm/angiosperm) ratios were plotted as indicators of the source of vascular plant (Hedges and Mann, 1979). The lignin-phenol vegetation index (LPVI) was also applied to study sources of vascular plant materials (Tareq et al., 2004; Sánchez-García et al., 2009). The 3,5Bd is used as an index of soil degradation processes, while the 3,5Bd/V indicated inputs of organic matter humification products sorbed to fine particles in soils (Houel et al., 2006).

2.6 Modelling to Distinguish Sources of OC

A binary mixing model was used to resolve the non-rock-derived biospheric (OC_{bio}) and petrogenic (OC_{petro}) OC (Galy et al., 2008). Then the radiocarbon composition of the bulk OC can be expressed as follows:

$$Fm \times TOC = Fm_{petro} \times OC_{petro} + Fm_{bio} \times OC_{bio} \quad (1)$$

$$TOC = OC_{bio} + OC_{petro} \quad (2)$$

where, Fm, Fm_{bio}, and Fm_{petro} are fraction modern values of bulk TOC, OC_{bio}, and OC_{petro}, respectively. OC_{bio} has different quantities of radioactive carbon (Fm> 0), while OC_{petro} does not contain radioactive carbon (Fm = 0) (Galy et al., 2008). So, equation (1) is further modified as:

$$Fm \times TOC = Fm_{bio} \times (TOC - OC_{petro}) \quad (3)$$

Thus, Fm_{bio} (slope) and OC_{petro} (intercept/slope) can be estimated by plotting Fm ×TOC versus TOC on an X–Y plot, while OC_{bio} is estimated by the offset between bulk TOC and OC_{petro}.

A Monte Carlo simulation model was applied to track the sources of the sedimentary TOC from C_3, C_4 plants, riverbank soil, river phytoplankton, and marine algae. Assuming that the endmember parameters ($\delta^{13}C$ and N/C) followed a normal distribution (mean ± standard deviation) for different OC sources in the study system (**Table S1**), the program was run in Python 3.8.2. Briefly, 4000 out of 1,000,000 random samples from the normal distribution of each end-member were taken in order to simultaneously optimize the following underdetermined system of linear equations:

$$\sum_1^i F_i = 1 \quad (4)$$

$$\sum_1^i F_i \times \delta^{13}C_i = \delta^{13}C_{sample} \quad (5)$$

$$\sum_1^i F_i \times (N/C)_i = (N/C)_{sample} \quad (6)$$

where F_i is the fraction of the i end-member and i = vascular C_3 plant, C_4 plant, soil OC, marine, and river phytoplankton, respectively. N/C, the inverse of C/N ratio, is used as a more sensitive end-member of terrestrial OC (Perdue and Koprivnjak, 2007; Li et al., 2017). The variation of the mean value for each end-member was less than 0.2‰ by randomly sampling each parameter value five times, ensuring the statistical stability of the model.

2.7 Carbon Burial Rate

The bulk carbon burial rate is calculated by the following equation:

$$\text{Bulk carbon burial rate} \quad (g\,C\,m^{-2}yr^{-1}) = TOC\,(\%) \times SAR\,(cm\,yr^{-1}) \times \text{bulk density}\,(g\,cm^{-3}) \times (1 - \text{porosity}) \times 100 \quad (7)$$

where, SAR was determined from ^{210}Pb chronology; the bulk density was assumed to be 1.5 g cm^{-3} in this region (Chen et al., 2006); TOC and porosity were the average values of 20-110 cm, 120-170 cm, 180-300 cm and the entire core.

The burial rate of each end-member was calculated by multiplying the bulk carbon burial rate and the fraction of each end-members from the mixing model. For example, the burial rate of lignin is calculated as:

$$\text{Lignin burial rate}\,(g\,\text{lignin}\,m^{-2}yr^{-1}) = \Lambda_8 \quad (mg\,\text{lignin}\,100\,mg^{-1}OC) \quad \times TOC\,(\%) \times SAR\,(cm\,yr^{-1}) \times \text{bulk density} \quad (g\,cm^{-3}) \times (1 - \text{porosity}) \quad (8)$$

2.8 Data Analyses

The Origin 2021 software was used to graph the figures. Statistical differences were calculated using one-way ANOVA. Statistically significant differences were discussed within the 95% confidence interval. Principle component analysis (PCA) was performed to discriminate for any other controlling variables linked with bulk and biomarker patterns in sediment samples with all parameters being mean-normalized.

3 RESULTS

3.1 Sediment Chronology

The cores displayed relatively low excess activities of ^{210}Pb ranging from 0.22 dpm g^{-1} to 2.62 dpm g^{-1} (1.33 ± 0.65 dpm g^{-1}, n=14) (**Figure 2** and **Table S2**). While grain size variation can generate an error in the downcore decay trend in relatively low excess activity samples, the core showed a supported ^{210}Pb level (from ^{226}Ra activity) that were relatively invariant downcore (2.16–2.86 dpm g^{-1}) (**Figure 2**). The surface mixed layer was around 20 cm with the depth below showing the sediment accumulation. The best fit exponential regression of excess ^{210}Pb activity (R^2 = 0.69, p<0.01) yielded a varied sedimentation rate (LSR) ranging from 1.71 cm yr^{-1} (210-250 cm) to 3.18 cm yr^{-1} (20-30 cm). The calculated geochronology dated back to 1893 for the deepest sample. Therefore, the core represents about 130 years of sediment deposition.

3.2 Bulk Organic Carbon/Nitrogen, Stable and Radiocarbon Isotopes

The TOC (%) varied from 0.43% to 1.43% (0.96 ± 0.22%, n=40) (**Figure 3A**). The TN ranged from 0.11% to 0.28% (0.24 ± 0.03%, n=40) (**Figure 3B**). A significant linear relationship between TN and TOC (R^2 = 0.49, p < 0.01) suggested that TN was derived predominantly from the organic origin. The C/N ratio varied from 2.27 to 9.33 (4.69 ± 1.18, n=40) (**Figure 3D**). The $\delta^{13}C$ ranged from -24.54 to -22.89‰ and showed three stages with different $\delta^{13}C$ features (**Figure 3C** and **Figure S1**). Between 1893 and 1957, the average $\delta^{13}C$ value was -23.08 ± 0.16‰. Between 1957 and 1980, the value showed a large variability (-23.59 ± 0.29‰), while after 1980, the average $\delta^{13}C$ decreased to -23.86 ± 0.34‰ (**Figure S1**), indicating an increased proportion of terrestrial OC. The $\Delta^{14}C$ value varied from -448.40‰ to -209.55‰ (-299.26 ± 66.89‰, n=20) (**Figure 3E** and **Figure S1**). The average $\Delta^{14}C$ value was

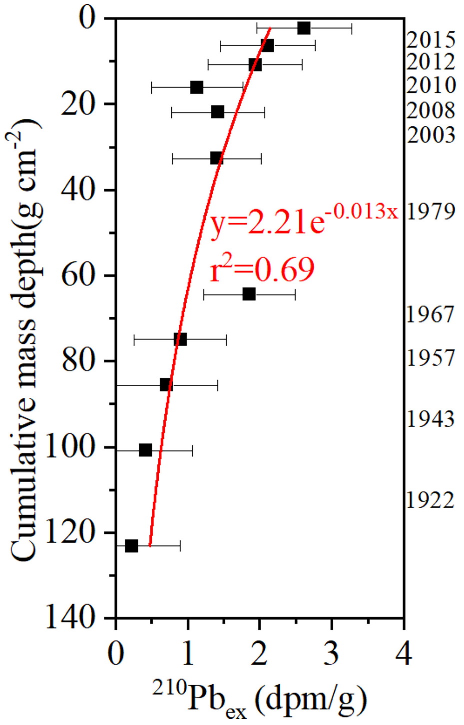

FIGURE 2 | The cumulative mass depth profile of excess ^{210}Pb ($^{210}Pb_{ex}$) of the sediment core. The right scale labeled the chronology.

-226.84‰ (n=6), -399.04‰ (n=3), and -316.88‰ (n=9) (**Figure S1**) in stage of 1893 to 1957, 1957 to 1980, and after 1980, respectively. Correspondingly, the average Fm in stages of 1893 to 1957, 1957 to 1980, and after 1980 were 0.78 (n=6), 0.61 (n=3), and 0.69 (n=9) (**Figure S1**), respectively.

3.3 Grain Size

The clay, silt and sand content of the core ranged from 11.58 to 35.6% (26.24 ± 5.82%, n=40), 60.36 to 74.56% (66.54 ± 3.34%, n=40), 0 to 16.2% (7.22 ± 4.63%, n=40), respectively (**Figure 3F** and **Figure S1**). The sediments were predominately fine-grained (<63 µm) that the sum of clay and silt ranged from 83.8% to 100%. The proportion of clay and silt were negatively correlated in all layers (R^2 = 0.61, p<0.01).

The median grain size (MGS) ranged from 5.83 to 26.9µm (9.88 ± 4.33µm, n=40) (**Figure 3F**). Before the 1960s, the MGS was relatively constant at a low value (6.90 ± 0.74, n=15), while they became more variable and showed relatively higher values (11.83 ± 4.61, n=25) after the 1960s. The MGS has a peak value around 2008. The correlation map between multiple correlation coefficient and numbers of end-member (EM) indicated that two EMs could fulfill the observed compositional variation required in EMA (Jiang et al., 2017) and explain the grain-size distribution pattern that the peak values were concentrated at 6.72 µm (EM 1), and 40.14 µm (EM 2), respectively. The EM1 and EM2 ranged from 36.91% to 97.42% (78.43 ± 14.78%, n=40), 2.58% to 63.09% (21.57 ± 14.78%, n=40), respectively (**Figure S2**).

3.4 Lignin-Phenols

The Λ_8 values ranged from 0.43 to 2.84 mg 100mg^{-1} OC (1.39 ± 0.54, n=40) (**Figure 4A**). There was a general increase in Λ_8 from the bottom to the surface sediment, that the average Λ_8 in stages of 1893 to 1957, 1957 to 1980, and after 1980 were 1.04 (n=13), 1.18 (n=6), 1.68 (n=21) mg 100mg^{-1} OC, respectively. This trend indicated an increasing accumulation of vascular plant derived OC. The 3,5Bd showed no significant changes with depth (p > 0.01) (**Figure 4B**). The average (Ad/Al)v values were 0.38 (n=13), 0.35 (n=6) and 0.26 (n=21), while the average (Ad/Al)s were 0.35 (n=13), 0.36 (n=6) and 0.23 (n=21) from 1893 to 1957, 1957 to 1980, and after 1980, respectively (**Figures 4C, D**). Their

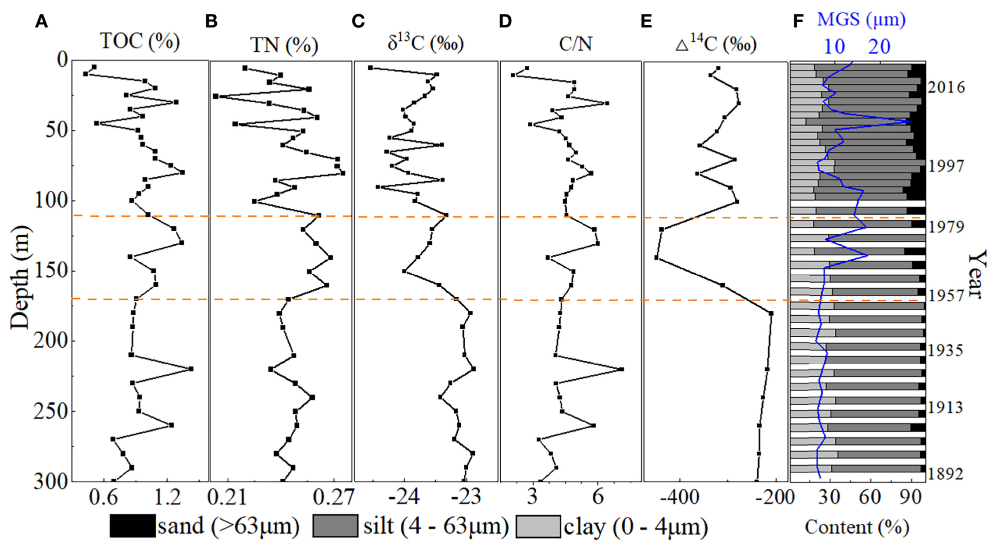

FIGURE 3 | Depth profiles of **(A)** TOC(%), **(B)** TN(%), **(C)** $\delta^{13}C$(‰), **(D)**C/N ratio, **(E)** $\Delta^{14}C$(‰), and **(F)** median grain size (MGS) and mineral content (%).

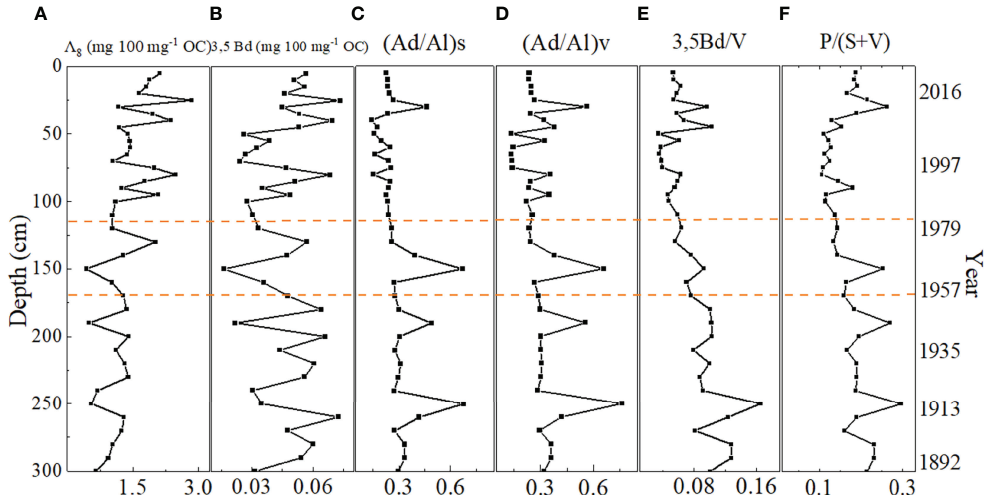

FIGURE 4 | Depth profiles of **(A)** Λ_8(mg 100mg^{-1} OC), **(B)** 3,5Bd (mg 100mg^{-1} OC), **(C)** the (Ad/Al)s ratio, **(D)** (Ad/Al)v ratio, **(E)** 3,5Bd/V ratio, and **(F)** P/(S+V) ratio in sediment cores of the PRE.

insignificant depth variations (p<0.01) indicated insignificant degradation, or that the majority of bioavailable lignin has been consumed prior to delivery to the ocean (Seidel et al., 2015). The ratios of 3,5Bd/V and P/(S+V) ranged from 0.03 to 0.17 (0.08 ± 0.03, n=40), 0.11 to 0.3 (0.17 ± 0.05, n=40) with slight increase with depths (**Figures 4E, F**).

3.5 Modelling Results and Carbon Burial Rates

The modelling results showed historical variability in the Fm_{bio}, OC_{petro} (%), OC_{bio} (%), OC_{bio}/OC (%) in the PRE sediments (**Figure 5A** and **Table 1**). The Fm_{bio} (0.79) values in 1957-1980 were smaller than before 1980 (0.63). Conversely, the OC_{petro} value (0.03) in 1957-1980 was three times higher than before 1980 (0.01), indicating more petrogenic and less biospheric OC input during 1957-1980.

The comprehensive five-end-member simulation showed that the fraction of C_3 plants (F_{C3}), riverbank soil (F_{soil}), riverine phytoplankton ($F_{riverine\ phytoplankton}$), marine algae ($F_{marine}$) and, C_4 plants (F_{C4}) were 17 ± 3%, 17 ± 2%, 22 ± 1%, 35 ± 10%, 10 ± 3%, respectively (**Figure 5B** and **Table 2**). The fraction of total terrestrial OC (F_{terr}= F_{C3}+F_{soil}+$F_{riverine\ phytoplankton}$+$F_{C4}$) was 65 ± 10%. The F_{C3} in 1893-1957 was 14 ± 3%, which was smaller than 1957-1980 (20 ± 2%) and 1980-2016 (19 ± 2%). The F_{C4} in 1980-2016 was lower than 1957-1980(13 ± 2%) and 1897-1957(10 ± 4%). This indicated a change in plant contribution from C_4 plants to C_3 plants from the bottom to the surface sediment. The F_{soil} (19 ± 2%) in 1957-1980 were larger than the average value (17 ± 2%), while the F_{marine} (27 ± 6%) in 1957-1980 was smaller than the average value (35 ± 10%) in the entire core.

The PCA biplot included 17 normalized variables (**Figure 5C**). The first two components explained 52.5% of the sedimentary OC (PC1: 36.1% and PC2: 16.4%). The plot showed significant depth variations of the distribution and preservation of sedimentary OC across different temporal scales (**Figure 5B**). Most of the samples above 110cm (exclude 30cm) were located in Quadrant II and III, and the samples between 120 and 180cm (exclude 180cm) were located in Quadrants III and IV, while most of the deeper (190-300cm) samples were located in Quadrants I and IV.

The bulk OC burial rate increased from 1893-1957 (94 ± 22 gC m^{-2} yr^{-1}) to 1957-1980 (138 ± 24 gC m^{-2} yr^{-1}), but decreased after 1980 (151 ± 44 gC m^{-2} yr^{-1}) (**Table 3**). The trends of the end-member burial rates were similar to the bulk OC, which were increased first and then decreased except the burial rate of marine algae (**Table 3**).

4 DISCUSSION

4.1 Historical Changes of OC Sources in the PRE Sediment

The significant correlation between δ^{13}C and C/N (R^2 = 0.55, p< 0.01, **Figure 6A**) suggested mixed source input from terrestrial and marine OC. The MGS and δ^{13}C signatures were invariable in the bottom of the sediment core (> 150cm), but became coarser and more negative at discrete intervals in upper parts of the core (above 150cm) (**Figures 3C, F**) indicating a shift from marine plankton with younger ^{14}C age to terrestrial derived OC which was older (**Figures 3E, 5A**). This was likely due to a transition (~ the 1980) from steady-state deposition with lower sediment accumulation rate (**Figure 2** and **Table S2**), to an environment influenced by both stronger anthropogenic and climate disturbance in the modern PRE (Yuan et al., 2019) with enhanced sediment accumulation rate (**Figure 2** and **Table S2**) (Owen and Lee, 2004).

More than 100 red tides have been reported in the PRE since the 1970s, and their frequency has increased in recent years due to human influences (Jia and Peng, 2003; Hu et al., 2008). However, the average marine sourced OC derived from the Monte Carlo model decreased by 20% during 1980-2016 than that from 1893-1957 (**Table 2**). This may be related to the high degradation rates of

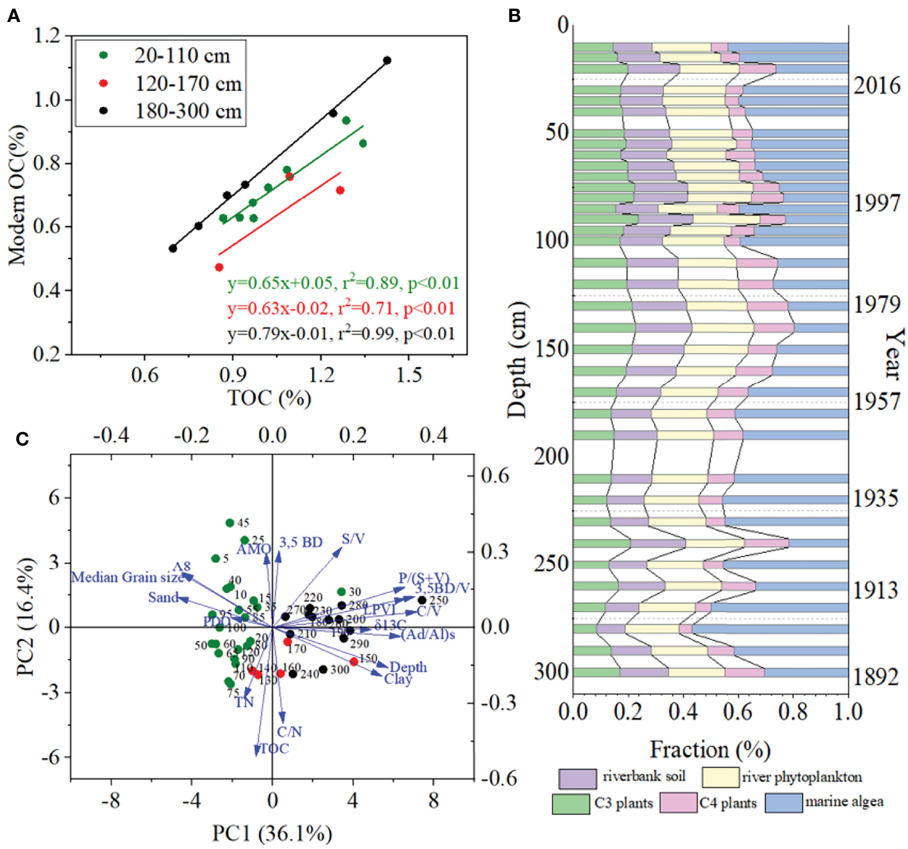

FIGURE 5 | **(A)** A binary plot used to determine OC_{petro} concentration in bulk sediments by plotting Fm of bulk TOC × TOC (%) vs. TOC (%). The solid lines represented the best linear fit of the three periods. The slope represented the fraction of modern value of biospheric OC (Fm_{bio}), while the intercept on x-axis represented the content of petrogenic OC (OC_{petro}) in sediments. **(B)** Fraction of OC sources from five end-members based on Monte Carlo simulation of the PRE sediment core. **(C)** Principal component analyses of parameters in this study.

TABLE 1 | Historical changes of Fm_{bio}, OC_{petro} (%), OC_{bio} (%), and OC_{bio}/OC (%) in the PRE sediment.

Depth (cm)	Stage	Fm_{bio}	OC_{petro} (%)	OC_{bio} (%)	OC_{bio}/OC(%)
20-110	1980-2016	0.65	–	–	–
120-170 cm	1957-1980	0.63	0.03	1.06	97.2
180-300 cm	1893-1957	0.79	0.01	0.91	98.9
120-300	1893-1980	0.71	0.02	0.99	98.1

TABLE 2 | Fraction of C_3 plants, riverbank soil, riverine phytoplankton, C_4 plants, marine algae and total terrestrial OC in PRE sediments.

	Stage	F_{C3} (%)	F_{soil} (%)	$F_{riverine\ phytoplankton}$ (%)	F_{C4} (%)	F_{marine} (%)	F_{terr} (%)
20-110 cm	1980-2016	19 ± 2	17 ± 1	23 ± 1	8 ± 3	33 ± 6	67 ± 6
120-170 cm	1957-1980	20 ± 2	19 ± 2	22 ± 1	13 ± 2	27 ± 6	73 ± 6
180-300 cm	1893-1957	14 ± 3	15 ± 2	20 ± 2	10 ± 4	41 ± 9	59 ± 9
Entire core	1893-2016	17 ± 3	17 ± 2	22 ± 1	10 ± 3	35 ± 10	65 ± 10

TABLE 3 | Burial rate (g C m^{-2} yr^{-1}) of the TOC and each end-member.

Core depth (cm)	Stage	TOC	OC_{petro}	C_3 plants	Riverbank soil	River phytoplankton	Marine algea	C_4 plants	Lignin
20-110	1980-2016	136 ± 39	–	26	23	31	44	12	2.3
120-170	1957-1980	138 ± 24	4.2	28	26	31	37	18	1.8
180-300	1893-1957	94 ± 22	0.9	13	14	19	38	9	1.0
Entire core	1893-2016	126 ± 29	2.5	21	21	28	44	12	1.8

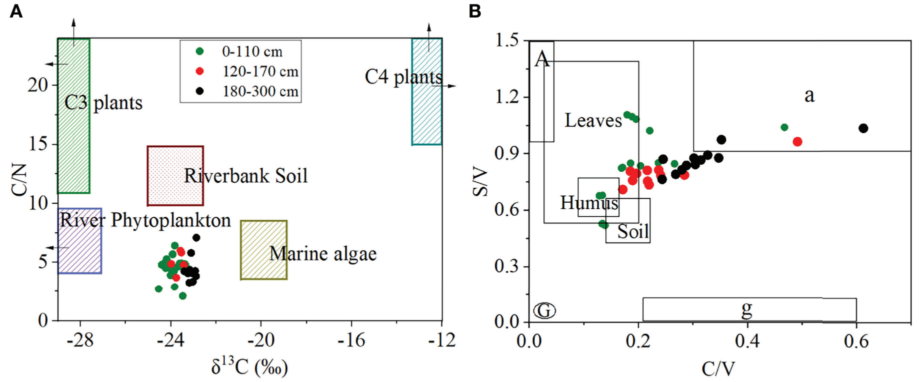

FIGURE 6 | Source plot of the sedimentary OC in the PRE based on **(A)** $\delta^{13}C$ and C/N; **(B)** C/V and S/V. G=woody gymnosperm, g=nonwoody gymnosperm, A=woody angiosperm and a=nonwoody angiosperm.

marine algae enriched in labile compositions such as carbohydrates, sugars, amino acids, and low-molecular-weight organic acids (Hardison et al., 2013). Instead, the vascular plant biomarker of lignin did not show much degradation during the burial process (**Figures 4C, D**) that the variations were more induced by concentration changes with continuous input of relatively stable terrestrial OC, which were partly diluted by the marine-derived OC as was indicated from a lack of correlation between lignin-phenol abundance and TOC (R^2 = 0.02, p<0.01).

Sources of vascular plant derived OC changed during the sediment accumulation. In general, the angiosperms (woody or non-woody tissues) contain a large amount of syringyl phenols. Therefore, the bottom depths with relatively high S/V values (0.83 ± 0.14, n=40) (**Figure 6B**) suggested an important fraction of lignin originating from angiosperm plants with higher LPVI (**Table S3**) than that of gymnosperms (Tareq et al., 2004). The surface sediments, instead, tended to be sourced from leaves, humus, and soil (**Figure 6B**) as a result of increased soil erosion induced terrestrial plant input. The average LPVI decreased from the bottom to the surface sediment also supported a change from angiosperms to gymnosperms (Tareq et al., 2004; Li et al., 2017) that rapid urbanization has caused such loss in the angiosperm-rich farmland since the 1980s (Zhang et al., 2008) (**Table S3**).

4.2 Biospheric and Petrogenic OC in the PRE Sediment

The sediment record showed a significant input of old carbon during 1957-1980 (**Figure 3**; **Figure 7**), which corresponded to lower Fm and OC_{bio} values and higher $\Delta^{14}C$ and OC_{petro} values (**Table 1**). It happened that this period had a higher TOC value (**Figure S1**) and terrestrial input (73%, **Table 2**). This may be caused by hydrodynamic sorting of riverine OC containing significant eroded soil with more negative $\Delta^{14}C$ and older apparent ages (Wei et al., 2010). The significant correlation between MGS and $\Delta^{14}C$ values (R^2 = 0.52, p<0.01, **Figure S3**) illustrated the importance of hydrodynamics on the transport and sorting of different grain size fractions, which should be considered in the aging processes, particularly in the estuary and continental shelf characterizing by strong hydrodynamic gradients (Bao et al., 2018a). Specifically, OC in the finer fraction was the youngest, with ^{14}C ages and OC_{petro} increasing in the coarser fraction. So, the OC was preferentially associated with fine-grained, large-surface-area minerals providing stronger protection against degradation (Ausín et al., 2021). The young OC with less negative $\delta^{13}C$ values (**Figure S1**) were mainly from marine inputs during 1893-1957. Selective removal of labile marine OC was expected leading to more negative $\Delta^{14}C$ and $\delta^{13}C$ values, *via* preferential degradation of ^{13}C-enriched, labile organic components afterwards. Correspondingly, the finer EM1 (6.72 μm) was dominant (78.4 ± 14.8%, n=40) (**Figure S2**) in the bottom of the PRE sediments, which was beneficial to the OC preservation. Thus, the ^{14}C age was younger with higher EM1.

The average Fm_{bio} value (0.71) of the PRE is the lowest in coastal China among Bohai, Yellow Sea, and East China Sea (**Table 4**), but closer to that of the Yellow River POC (0.61), indicating older ages of biogenic OC in the PRE. The Yellow River generally has a large amount of pre-aged POC sourced from the Loess Plateau where distributes thick loess-paleosol deposits, with serious soil erosion and sparse vegetation (Eliassen, 2020). In comparison, the upper and middle reaches of the PRE drain the karst morphology areas with the carbonate rocks being the dominant lithology (Wu et al., 2020). The weathering rate of carbonate rocks is more than an order of magnitude higher than that of silicate rocks (Meybeck, 1987). As the carbonate rock weathers, the pre-aged materials including dissolved inorganic carbon are released into the river (Liu et al., 2017). Phytoplankton thus synthesize such old dissolved inorganic carbon resulting in biogenic OC with older ages and low Fm_{bio} values (**Table 4**). The relatively lower Fm_{bio} values have also been found in some other fluvial systems such as in the Mackenzie River shelf (**Table 4**). Warming and associated permafrost thaw exposed older biogenic OC with less OC_{petro} and lower Fm_{bio} accumulated in marine sediments (Hilton et al., 2015). Therefore, the relatively low Fm_{bio} composition in these aquatic ecosystems were attributed to the contribution from pre-aged OC in the drainage basin. As a result, the OC_{petro} contributed to 2% of TOC in the PRE. The ratio can be as low as 1% in the East China Sea sand area, and as high as 87% in the

TABLE 4 | Comparison of Fm_{bio}, OC_{petro}, OC_{bio} and OC_{petro}/TOC values in the sediments between the PRE and other studies.

Regions	Fm_{bio}	OC_{petro}	OC_{bio}	OCpetro/ TOC (%)	Reference
PRE	0.71	0.02	0.99	2	This study
Central Bohai Sea mud deposits	0.84	0.087	0.51	15	(Zhao et al., 2021)
Bohai Sea	0.75	0.013	0.38	3	(Bao et al., 2018b)
East China Sea	0.74	0.051	0.40	11	(Kao et al., 2003; Li et al., 2012; Wu et al., 2013; Kao et al., 2014; Bao et al., 2018b)
North Yellow Sea	0.86	0.030	0.48	6	(Bao et al., 2018b)
Southern Yellow Sea	0.82	0.041	0.51	7	(Bao et al., 2018b)
Shandong Peninsula mud deposits	0.93	0.088	0.66	12	(Zhao et al., 2021)
South Yellow Sea mud deposits	0.86	0.076	0.81	9	(Zhao et al., 2021)
Bohai and Yellow Seas sand area	0.78	0.015	0.32	4	(Zhao et al., 2021)
Changjiang Estuary mobile-muds	0.78	0.095	0.44	18	(Zhao et al., 2021)
Zhe-Min coastal mobile-muds	0.71	0.018	0.59	3	(Zhao et al., 2021)
southwest off the Cheju Island	0.82	0.040	0.52	7	(Zhao et al., 2021)
East China Sea sand area	0.68	0.002	0.30	1	(Zhao et al., 2021)
Yellow river POC	0.61	0.017	0.97	2	(Tao et al., 2015)
southeast Alaskan fjords	1.01	0.34	0.05	87	(Walinsky et al., 2009; Cui et al., 2016)
British Columbia fjords	1.11	0.26	0.70	27	(Smittenberg et al., 2004)
New Zealand fjords	0.96	0.30	2.43	11	(Smith et al., 2015)
US West Coastal	0.93	0.19	1.62	10	(Blair et al., 2003; Komada et al., 2005; White, 2006; Mollenhauer and Eglinton, 2007; Drenzek et al., 2009; Wakeham et al., 2009; Griffith et al., 2010; Feng et al., 2013)
Mackenzie River shelf	0.38	0.17	1.23	12	(Goñi et al., 2005; Drenzek et al., 2007; Hilton et al., 2015)
North Gulf of Mexico	0.79	0.09	0.92	9	(Goñi et al., 1998; Gordon and Goñi, 2003; Gordon and Goñi, 2004)
Amazon River Coast	0.84	0.03	0.62	5	(Aller and Blair, 2006; Williams et al., 2015)

southeast Alaskan fjords (**Table 4**). But on average, the OC_{petro}/TOC in the PRE was lower than the mean values of 13 ± 18% in global aquatic systems.

4.3 Drivers for the Historical Changes of OC Burial Rate

4.3.1 The Climate Oscillation Effect

The climate oscillation associated with rainfall intensity affected the frequency and magnitude of soil erosion (Starkloff and Stolte, 2014; Li and Fang, 2016; Zhang et al., 2022) and sediment accumulation rate. A significant increase in the sedimentary grain size in the upper core around 2008 (**Figure 3F**) suggested stronger hydrodynamic conditions due to pulsed flooding events this year with significant sediment delivery (Owen and Lee, 2004). In fact, a big flooding event occurred in almost every other year between 2000 and 2011 due to typhoon and flood impacts in the PRE (Yang et al., 2015). Strong rainfall-runoff processes would in turn erode deep soil and vascular plant OC from the drainage basin in pulses (Hao and Lu, 2021), which cause a large amount of old OC to enter the river and further the PRE. As a result, the riverine POC was dominated by aquatic organisms during the low-flow periods, while the terrigenous POC (mainly from soil minerals and degraded plant debris) became dominant during high-flow periods. The pulsed (Ad/Al)v and (Ad/Al)s ratio that appeared during this time proved the input of highly degraded vascular plant materials during the flooding erosion. The increased transportation capacity of rivers could then accelerate POC transportation with less residence time for POC oxidation and high burial efficiency (Blair and Aller, 2012). Therefore, the export of OC_{petro} and the escape of OC_{bio} from oxidation by rapid transport along rivers resulted in subsequent increase in OC burial on adjacent margins in the PRE. In fact, the 1957-1980 period witnessed 4.6 times higher petrogenic OC burial rate than before with a significant decrease of $\Delta^{14}C$ from -218.6 ± 81.8‰ (1893-1957) to -395.3 ± 31.8 ‰ (1957-1980) (**Figure 7** and **Table 3**).

The large variability of summer precipitation may easily trigger floods and droughts in the Pearl River basin that a correlation (R^2 = 0.89) has been found between precipitation and surface runoff (Luo et al., 2016). As global climate phenomenon, the PDO have been reported to be closely related to precipitation and droughts frequency in China over the last century (Chan and Zhou, 2005; Duan et al., 2013; Yang et al., 2017a; Yang et al., 2017b). However, the AMO may act as a key pacemaker that the western tropical Pacific multidecadal climate variability is forced by the AMO instead of PDO in interdecadal time scales over the last century (Sun et al., 2017; Zheng and Wang, 2021). In this study, the correlations between terrestrial OC parameters (e.g., F_{terr}, **Table 5**) and both 7-year running mean of climate oscillation

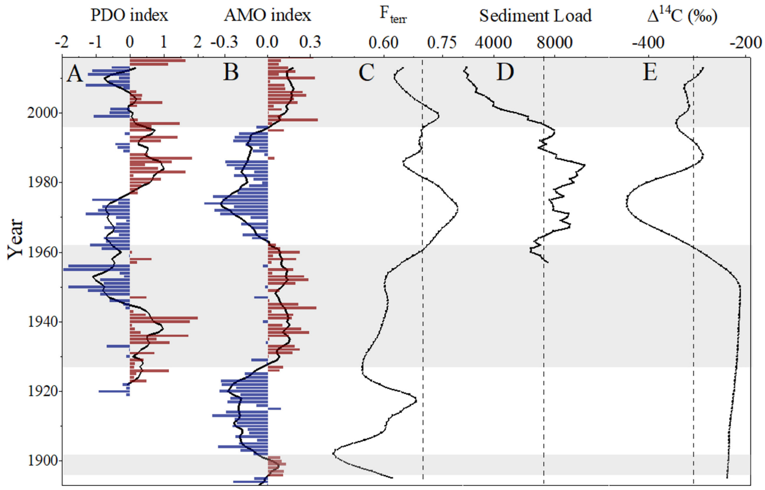

FIGURE 7 | **(A)**Pacific Decadal Oscillation (PDO) index; **(B)** Atlantic Multidecadal Oscillation (AMO) index; **(C)** Fraction of total terrestrial OC (F_{terr}, %) from Monte Carlo simulation; **(D)** Sediment load (10^4 t yr^{-1}) of Pearl River, modified from Wei et al. (2020); and **(E)** $\Delta^{14}C$ (‰). The interpolation method was applied for data processing. The values for the PDO index were taken from University of Washington (http://jisao.washington.edu/pdo/PDO.latest) (Duan et al., 2013). The AMO index is downloaded from Earth System Research Laboratory (http://www.esrl.noaa.gov/psd/data/correlation/amon.sm.data). The bars were annual index value. The black curves represented 7 year running mean value in **(A, B)** The monthly mean global average sea surface temperature (SST) anomalies have been removed to separate this pattern of variability from any global warming signal that may be present in the data (Mantua et al., 1997).

index were not significantly correlated (AMO, R = 0.28, p <0.01; PDO, R=0.27, p <0.01) (**Figure 7** and **Table 5**) through the whole core. However, there is a significant correlation between F_{terr} and PDO than that with AMO before 1957 (R=0.43, p<0.01). Instead, the AMO and F_{terr} were significantly correlated between 1957-1980 (R=-0.93, p<0.01), but not before 1957 (R=-0.10, p=0.43) and after 1980 (R=-0.20, p=0.27), indicating that the climate effect on the OC burial has changed from PDO before 1957, to AMO between 1957 and 1980 in the PRE. The reason might be that during the negative phase of AMO (e.g., 1957-1980), humid climate condition and more typhoon events in PRE intensified the washout of riverbanks and surrounding soils, hence more terrestrial (F_{terr}) including petrogenic OC were transported to the sediments (**Figure 7** and **Table 5**). At the positive phase of AMO, cold climate and less precipitation, in contrast, would result in less soil erosion, delivery and burial of terrestrial and petrogenic OC. There was no significant correlation between the F_{terr} and the climate oscillation index (AMO, R = 0.20, p =0.27; PDO, R=0.31, p=0.08) after 1980, which is mostly related to the beginning of Economic Reform and Open Up, suggesting the dominate influence from human perturbations.

4.3.2 The Impact From Human Perturbations

Deforestation tended to destabilize slopes and increased soil erosion rates (Owen and Lee, 2004). With the explosive growth of population and gross domestic product (GDP) in the Pearl River basin (**Figure 8**), large areas have been deforested since the 1950s (Liu et al., 2014). Correspondingly, the average Λ_8 value increased from 1.02 (n=10) before 1950 to 1.52 (n=30) mg 100 mg^{-1} OC after 1950 (**Figure 8**) with 1.6 times increase in the lignin burial rates from 1893-1957 (1.0 g lignin m^{-2} yr^{-2}) to 1980-2016 (2.4 g lignin m^{-2} yr^{-2}) (**Table 3**). The obvious discontinuities displayed on Λ_8 were also evidence of deforestation activities (Bélanger et al., 2017). In Foshan, a city on the coast of PRE, approximately 60% of the newly built-up land was converted from pond, farmland, forest, and shrub during 1988–2003, and the forest and shrub were then changed to farmland to compensate the farmland loss (Yang et al., 2015). Eventually, a shift from marine plankton to terrestrial plants was

TABLE 5 | Correlation between OC and climate oscillation index based on 7 year running mean value.

Correlation (R)	$\Delta^{14}C$	F_{terr}	F_{soil}	Sediment load
AMO	**0.35 (p<0.01)**	**-0.28 (p<0.01)**	**-0.27 (p<0.01)**	**-0.81(p<0.01)**
PDO	-0.17 (p=0.07)	**-0.27 (p<0.01)**	**-0.26 (p<0.01)**	0.30 (p=0.02)
AMO after 1980	0.15 (p=0.41)	-0.20 (p=0.27)	-0.17 (p=0.34)	**-0.90 (p<0.01)**
AMO 1957-1980	**0.98 (p<0.01)**	**-0.93 (p<0.01)**	**-0.92 (p<0.01)**	**-0.65 (p<0.01)**
AMO before 1957	**0.35 (p<0.01)**	-0.10 (p=0.43)	-0.10 (p=0.45)	-
PDO after 1980	-0.20 (p=0.26)	0.31 (p=0.08)	0.28 (p=0.10)	**0.85 (p<0.01)**
PDO 1957-1980	-0.13 (p=0.56)	-0.15 (p=0.52)	-0.17 (p=0.46)	0.05 (p=0.82)
PDO before 1957	0.14 (p=0.30)	**-0.43 (p<0.01)**	**-0.42 (p<0.01)**	-

Values in bold indicated significant correlations (p<0.01).

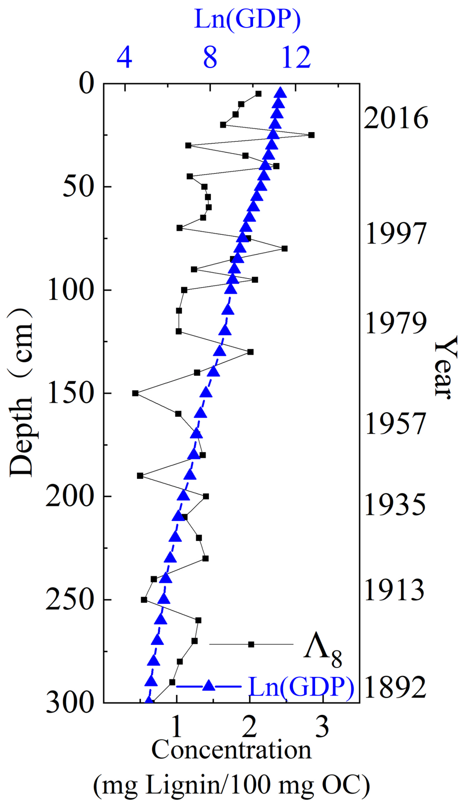

FIGURE 8 | Depth profiles of Λ_8 and Ln(GDP) in sediment cores of the PRE.

observed from the bottom to surface sediments, in agreement with significant older radiocarbon signature (**Figure 5A**) with increased MGS in the study (**Figure 3F**). The dam construction on Pearl rivers have greatly modified the transport of sediment since mid-1980s (Dai et al., 2008; Wei et al., 2020). The decrease of TOC (**Figure 3A**) and F_{terr} (**Figure 7C**), as well as significant correlation between sediment load and F_{terr} ($R=0.64$, $p<0.01$) supported that dam construction has reduced delivery of terrestrial derived OC since the 1980s. The unpredictable human disturbance also likely resulted in dynamic source and fate of OC and unresolved OC_{petro} (**Figure 5A** and **Table 1**). So, the OC cycle under the varied extent of human perturbations in the PRE is definitely important to monitor in the future.

5 CONCLUSIONS

The study synthesized marine sediment records spanning the past 130 yr to decipher the sources and burial rate of OC in the PRE. The results suggested three stages of 1893-1957, 1957-1980 and 1980-2016 with distinct OC features. The 1893-1957 stage was more affected by the PDO with burial of younger marine derived OC. The input of petrogenic OC is increasing during the 1957-1980 that the burial rate of OC_{petro} was 4.6 times higher than before due to input of eroded older soil OC and marine derived OC assimilated from weathered old dissolved inorganic carbon. Additionally, a significant correlation between the F_{terr} and AMO was observed that the increasing frequency of the negative AMO events. After 1980, there was no significant relationship between F_{terr} and the two climate indices suggesting a shift to human perturbation such as deforestation and dam construction likely affecting the OC burial in the region. A transition stage from low sediment accumulation rate to a relatively higher deposition environment was observed after ca. ~1980s in the PRE. Therefore, it is important to understand the effects of climate oscillation and human perturbation on the OC burial in the dynamic PRE to better understand its role in current climate change.

DATA AVAILABILITY STATEMENT

The original contributions presented in the study are included in the article/**Supplementary Material**. Further inquiries can be directed to the corresponding author.

AUTHOR CONTRIBUTIONS

Conceptualization: XL and CW. Methodology: WL, XL, and CW. Investigation: WL, XZ, CS, TN, and YH. Visualization: WL and XL. Funding acquisition: XL. Supervision: XL and CW. Writing – original draft: WL, XL, and CW. Writing – review and editing: WL, XL, XZ, CS, TN, YH, and CW. All authors contributed to the article and approved the submitted version.

FUNDING

This work was supported by Southern Marine Science and Engineering Guangdong Laboratory (Guangzhou) (GML2019ZD0210, K19313901), National Natural Science Foundation of China (42076029, 41720104001), Shenzhen Key Laboratory of Marine Archaea Geo-Omics, Southern University of Science and Technology (ZDSYS20180208184349083) and Guangxi Key Laboratory of Marine Disaster in the Beibu Gulf, Beibu Gulf University (No.2020KF01).

ACKNOWLEDGMENTS

We would like to thank Wenxiu Wang and Chuanlun Zhang for providing sediment samples, Hanchao Jiang and Qiaoqiao Guo for grain size measurement and analysis, Daidu Fan and Yijing Wu for the 210 Pb measurement and analysis, and the reviewers for the constructive comments.

SUPPLEMENTARY MATERIAL

The Supplementary Material for this article can be found online at: https://www.frontiersin.org/articles/10.3389/fmars.2022.848757/full#supplementary-material

REFERENCES

Aller, R. C., and Blair, N. E. (2006). Carbon Remineralization in the Amazon–Guianas Tropical Mobile Mudbelt: A Sedimentary Incinerator. *Continent. Shelf. Res.* 26, 2241–2259. doi: 10.1016/j.csr.2006.07.016

Appleby, P. G., and Oldfield, F. (1978). The Calculation of Lead-210 Dates Assuming a Constant Rate of Supply of Unsupported 210Pb to the Sediment. *CATENA* 5, 1–8. doi: 10.1016/S0341-8162(78)80002-2

Ausín, B., Bruni, E., Haghipour, N., Welte, C., Bernasconi, S. M., and Eglinton, T. I. (2021). Controls on the Abundance, Provenance and Age of Organic Carbon Buried in Continental Margin Sediments. *Earth Planet. Sci. Lett.* 558, 1–10. doi: 10.1016/j.epsl.2021.116759

Bao, R., Uchida, M., Zhao, M., Haghipour, N., Montlucon, D., McNichol, A., et al. (2018a). Organic Carbon Aging During Across-Shelf Transport. *Geophys. Res. Lett.* 45, 8425–8434. doi: 10.1029/2018GL078904

Bao, R., van der Voort, T. S., Zhao, M., Guo, X., Montluçon, D. B., McIntyre, C., et al. (2018b). Influence of Hydrodynamic Processes on the Fate of Sedimentary Organic Matter on Continental Margins. *Global Biogeochem. Cycle.* 32, 1420–1432. doi: 10.1029/2018GB005921

Bélanger, É, Lucotte, M., Moingt, M., Paquet, S., Oestreicher, J., and Rozon, C. (2017). Altered Nature of Terrestrial Organic Matter Transferred to Aquatic Systems Following Deforestation in the Amazon. *Appl. Geochem.* 87, 136–145. doi: 10.1016/j.apgeochem.2017.10.016

Bianchi, T. S., and Allison, M. A. (2009). Large-River Delta-Front Estuaries as Natural "Recorders" of Global Environmental Change. *Proc. Natl. Acad. Sci.* 106, 8085–8092. doi: 10.1073/pnas.0812878106

Bianchi, T. S., Cui, X. Q., Blair, N. E., Burdige, D. J., Eglinton, T. I., and Galy, V. (2018). Centers of Organic Carbon Burial and Oxidation at the Land-Ocean Interface. *Organ. Geochem.* 115, 138–155. doi: 10.1016/j.orggeochem.2017.09.008

Bianchi, T. S., Mitra, S., and McKee, B. A. (2002). Sources of Terrestrially-Derived Organic Carbon in Lower Mississippi River and Louisiana Shelf Sediments: Implications for Differential Sedimentation and Transport at the Coastal Margin. *Mar. Chem.* 77, 211–223. doi: 10.1016/S0304-4203(01)00088-3

Blair, N. E., and Aller, R. C. (2012). The Fate of Terrestrial Organic Carbon in the Marine Environment. *Ann. Rev. Mar. Sci.* 4, 401–423. doi: 10.1146/annurev-marine-120709-142717

Blair, N. E., Leithold, E. L., Ford, S. T., Peeler, K. A., Holmes, J. C., and Perkey, D. W. (2003). The Persistence of Memory: The Fate of Ancient Sedimentary Organic Carbon in a Modern Sedimentary System. *Geochim. Cosmochim. Acta* 67, 63–73. doi: 10.1016/S0016-7037(02)01043-8

Breithaupt, J. L., Smoak, J. M., Bianchi, T. S., Vaughn, D. R., Sanders, C. J., Radabaugh, K. R., et al. (2020). Increasing Rates of Carbon Burial in Southwest Florida Coastal Wetlands. *J. Geophys. Res.: Biogeosci.* 125 (2), 1–25. doi: 10.1029/2019jg005349

Canuel, E. A., and Hardison, A. K. (2016). Sources, Ages, and Alteration of Organic Matter in Estuaries. *Ann. Rev. Mar. Sci.* 8, 409–434. doi: 10.1146/annurev-marine-122414-034058

Chan, J. C. L., and Zhou, W. P. D. O. (2005). ENSO and the Early Summer Monsoon Rainfall Over South China. *Geophys. Res. Lett.* 32 (8), 1–5. doi: 10.1029/2004GL022015

Chen, S.-J., Luo, X.-J., Mai, B.-X., Sheng, G.-Y., Fu, J.-M., and Zeng, E. Y. (2006). Distribution and Mass Inventories of Polycyclic Aromatic Hydrocarbons and Organochlorine Pesticides in Sediments of the Pearl River Estuary and the Northern South China Sea. *Environ. Sci. Technol.* 40, 709–714. doi: 10.1021/es052060g

Chen, Z., Nie, T., Zhao, X., Li, J., Yang, B., Cui, D., et al. (2022). Organic Carbon Remineralization Rate in Global Marine Sediments: A Review. *Reg. Stud. Mar. Sci.* 49, 102112. doi: 10.1016/j.rsma.2021.102112

Clark, K. E., Hilton, R. G., West, A. J., Malhi, Y., Gröcke, D. R., Bryant, C. L., et al. (2013). New Views on "Old" Carbon in the Amazon River: Insight From the Source of Organic Carbon Eroded From the Peruvian Andes. *Geochem. Geophys. Geosyst.* 14, 1644–1659. doi: 10.1002/ggge.20122

Cui, X. Q., Bianchi, T. S., Jaeger, J. M., and Smith, R. W. (2016). Biospheric and Petrogenic Organic Carbon Flux Along Southeast Alaska. *Earth Planet. Sci. Lett.* 452, 238–246. doi: 10.1016/j.epsl.2016.08.002

Dai, S. B., Yang, S. L., and Cai, A. M. (2008). Impacts of Dams on the Sediment Flux of the Pearl River, Southern China. *CATENA* 76 (1), 36–43. doi: 10.1016/j.catena.2008.08.004

Dalzell, B. J., Filley, T. R., and Harbor, J. M. (2005). Flood Pulse Influences on Terrestrial Organic Matter Export From an Agricultural Watershed. *J. Geophys. Res.: Biogeosci.* 110 (G2), 1–14. doi: 10.1029/2005jg000043

Drenzek, N. J., Hughen, K. A., Montluçon, D. B., Southon, J. R., Dos Santos, G. M., Druffel, E. R. M., et al. (2009). A New Look at Old Carbon in Active Margin Sediments. *Geology* 37, 239–242. doi: 10.1130/G25351A.1

Drenzek, N. J., Montluçon, D. B., Yunker, M. B., Macdonald, R. W., and Eglinton, T. I. (2007). Constraints on the Origin of Sedimentary Organic Carbon in the Beaufort Sea From Coupled Molecular 13C and 14C Measurements. *Mar. Chem.* 103, 146–162. doi: 10.1016/j.marchem.2006.06.017

Drinkwater, K. F., Miles, M., Medhaug, I., Otterå, O. H., Kristiansen, T., Sundby, S., et al. (2014). The Atlantic Multidecadal Oscillation: Its Manifestations and Impacts With Special Emphasis on the Atlantic Region North of 60°N. *J. Mar. Syst.* 133, 117–130. doi: 10.1016/j.jmarsys.2013.11.001

Duan, W. S., Song, L. Y., Li, Y., and Mao, J. Y. (2013). Modulation of PDO on the Predictability of the Interannual Variability of Early Summer Rainfall Over South China. *J. Geophys. Res-Atmos.* 118, 13008–13021. doi: 10.1002/2013JD019862

Eliassen, S. (2020). Soil Erosion and River Regulation With Special Reference to the Yellow River. *Environ. Geomorph. Landscape Conserv. Routled.* 17, 325–344. doi: 10.4324/9781003026563-18

Feng, X., Benitez-Nelson, B. C., Montluçon, D. B., Prahl, F. G., McNichol, A. P., Xu, L., et al. (2013). 14C and 13C Characteristics of Higher Plant Biomarkers in Washington Margin Surface Sediments. *Geochim. Cosmochim. Acta* 105, 14–30. doi: 10.1016/j.gca.2012.11.034

Galy, V., Beyssac, O., France-Lanord, C., and Eglinton, T. (2008). Recycling of Graphite During Himalayan Erosion: A Geological Stabilization of Carbon in the Crust. *Science* 322, 943–945. doi: 10.1126/science.1161408

Goñi, M. A., and Hedges, J. I. (1995). Sources and Reactivities of Marine-Derived Organic Matter in Coastal Sediments as Determined by Alkaline CuO Oxidation. *Geochim. Cosmochim. Acta* 59, 2965–2981. doi: 10.1016/0016-7037(95)00188-3

Goñi, M. A., Ruttenberg, K. C., and Eglinton, T. I. (1998). A Reassessment of the Sources and Importance of Land-Derived Organic Matter in Surface Sediments From the Gulf of Mexico. *Geochim. Cosmochim. Acta* 62, 3055–3075. doi: 10.1016/S0016-7037(98)00217-8

Goñi, M. A., Yunker, M. B., Macdonald, R. W., and Eglinton, T. I. (2005). The Supply and Preservation of Ancient and Modern Components of Organic Carbon in the Canadian Beaufort Shelf of the Arctic Ocean. *Mar. Chem.* 93, 53–73. doi: 10.1016/j.marchem.2004.08.001

Gordon, E. S., and Goñi, M. A. (2003). Sources and Distribution of Terrigenous Organic Matter Delivered by the Atchafalaya River to Sediments in the Northern Gulf of Mexico. *Geochim. Cosmochim. Acta* 67, 2359–2375. doi: 10.1016/S0016-7037(02)01412-6

Gordon, E. S., and Goñi, M. A. (2004). Controls on the Distribution and Accumulation of Terrigenous Organic Matter in Sediments From the Mississippi and Atchafalaya River Margin. *Mar. Chem.* 92, 331–352. doi: 10.1016/j.marchem.2004.06.035

Griffith, D. R., Martin, W. R., and Eglinton, T. I. (2010). The Radiocarbon Age of Organic Carbon in Marine Surface Sediments. *Geochim. Et. Cosmochim. Acta* 74, 6788–6800. doi: 10.1016/j.gca.2010.09.001

Hao, Y., and Lu, J. (2021). Teleconnection Between Climate Oscillations and Riverine Nutrient Dynamics in Southeast China Based on Wavelet Analysis. *Environ. Sci. Pollu. Res* 28, 41807–41820. doi: 10.1007/s11356-021-13715-x

Hardison, A. K., Canuel, E. A., Anderson, I. C., Tobias, C. R., Veuger, B., and Waters, M. N. (2013). Microphytobenthos and Benthic Macroalgae Determine Sediment Organic Matter Composition in Shallow Photic Sediments. *Biogeosciences* 10, 5571–5588. doi: 10.5194/bg-10-5571-2013

Hedges, J. I., Blanchette, R. A., Weliky, K., and Devol, A. H. (1988). Effects of Fungal Degradation on the CuO Oxidation Products of Lignin: A Controlled Laboratory Study. *Geochim. Cosmochim. Acta* 52, 2717–2726. doi: 10.1016/0016-7037(88)90040-3

Hedges, J. I., and Ertel, J. R. (1982). Characterization of Lignin by Gas Capillary Chromatography of Cupric Oxide Oxidation Products. *Anal. Chem.* 54, 174–178. doi: 10.1021/ac00239a007

Hedges, J. I., and Mann, D. C. (1979). The Characterization of Plant Tissues by Their Lignin Oxidation Products. *Geochim. Cosmochim. Acta* 43, 1803–1807. doi: 10.1016/0016-7037(79)90028-0

Hedges, J. I., and Parker, P. L. (1976). Land-Derived Organic Matter in Surface Sediments From the Gulf of Mexico. *Geochim. Cosmochim. Acta* 40, 1019–1029. doi: 10.1016/0016-7037(76)90044-2

Hilton, R. G., Galy, V., Gaillardet, J., Dellinger, M., Bryant, C., O'Regan, M., et al. (2015). Erosion of Organic Carbon in the Arctic as a Geological Carbon Dioxide Sink. *Nature* 524, 84–87. doi: 10.1038/nature14653

Houel, S., Louchouarn, P., Lucotte, M., Canuel, R., and Ghaleb, B. (2006). Translocation of Soil Organic Matter Following Reservoir Impoundment in Boreal Systems: Implications for *in Situ* Productivity. *Limnol. Oceanog.* 51, 1497–1513. doi: 10.4319/lo.2006.51.3.1497

Hu, J., Zhang, G., Li, K., Peng, PA, and Chivas, A. R. (2008). Increased Eutrophication Offshore Hong Kong, China During the Past 75 Years: Evidence From High-Resolution Sedimentary Records. *Mar. Chem.* 110, 7–17. doi: 10.1016/j.marchem.2008.02.001

Jiang, H., Guo, G., Cai, X., Thompson, J. A., Xu, H., and Zhong, N. (2016). Geochemical Evidence of Windblown Origin of the Late Cenozoic Lacustrine Sediments in Beijing and Implications for Weathering and Climate Change. *Palaeogeograph. Palaeoclimatol. Palaeoecol.* 446, 32–43. doi: 10.1016/j.palaeo.2016.01.017

Jiang, H., Wan, S., Ma, X., Zhong, N., and Zhao, D. (2017). End-Member Modeling of the Grain-Size Record of Sikouzi Fine Sediments in Ningxia (China) and Implications for Temperature Control of Neogene Evolution of East Asian Winter Monsoon. *PloS One* 12, e0186153. doi: 10.1371/journal.pone.0186153

Jia, G.-D., and Peng, P.-A. (2003). Temporal and Spatial Variations in Signatures of Sedimented Organic Matter in Lingding Bay (Pearl Estuary), Southern China. *Mar. Chem.* 82, 47–54. doi: 10.1016/S0304-4203(03)00050-1

Kao, S. J., Hilton, R. G., Selvaraj, K., Dai, M., Zehetner, F., Huang, J. C., et al. (2014). Preservation of Terrestrial Organic Carbon in Marine Sediments Offshore Taiwan: Mountain Building and Atmospheric Carbon Dioxide Sequestration. *Earth Surf. Dynamic.* 2, 127–139. doi: 10.5194/esurf-2-127-2014

Kao, S. J., Lin, F. J., and Liu, K. K. (2003). Organic Carbon and Nitrogen Contents and Their Isotopic Compositions in Surficial Sediments From the East China Sea Shelf and the Southern Okinawa Trough. *Deep. Sea. Res. Part II: Top. Stud. Oceanog.* 50, 1203–1217. doi: 10.1016/S0967-0645(03)00018-3

Komada, T., Druffel, E. R. M., and Hwang, J. (2005). Sedimentary Rocks as Sources of Ancient Organic Carbon to the Ocean: An Investigation Through Δ14C and δ13c Signatures of Organic Compound Classes. *Global Biogeochem. Cycle.* 19 (2), 1–10. doi: 10.1029/2004GB002347

Li, S., and Bates, G. T. (2007). Influence of the Atlantic Multidecadal Oscillation on the Winter Climate of East China. *Adv. Atmos. Sci.* 24, 126–135. doi: 10.1007/s00376-007-0126-6

Li, X. X., Bianchi, T. S., Allison, M. A., Chapman, P., Mitra, S., Zhang, Z. R., et al. (2012). Composition, Abundance and Age of Total Organic Carbon in Surface Sediments From the Inner Shelf of the East China Sea. *Mar. Chem.* 145, 37–52. doi: 10.1016/j.marchem.2012.10.001

Li, X. X., Bianchi, T. S., Allison, M. A., Chapman, P., and Yang, G. P. (2013). Historical Reconstruction of Organic Carbon Decay and Preservation in Sediments on the East China Sea Shelf. *J. Geophys. Res-Biogeosci.* 118, 1079–1093. doi: 10.1002/jgrg.20079

Li, X. X., Zhang, Z. R., Wade, T. L., Knap, A. H., and Zhang, C. L. L. (2017). Sources and Compositional Distribution of Organic Carbon in Surface Sediments From the Lower Pearl River to the Coastal South China Sea. *J. Geophys. Res-Biogeosci.* 122, 2104–2117. doi: 10.1002/2017JG003981

Li, W., Li, X., Mei, X., Zhang, F., Xu, J., Liu, C., et al. (2021). A Review of Current and Emerging Approaches for Quaternary Marine Sediment Dating. *Sci. Total. Environ.* 780, 1–19. doi: 10.1016/j.scitotenv.2021.146522

Li, Z., and Fang, H. (2016). Impacts of Climate Change on Water Erosion: A Review. *Earth-Sci. Rev.* 163, 94–117. doi: 10.1016/j.earscirev.2016.10.004

Li, Z., Wu, Y., Yang, L., Du, J., Deng, B., and Zhang, J. (2020). Carbon Isotopes and Lignin Phenols for Tracing the Floods During the Past 70 Years in the Middle Reach of the Changjiang River. *Acta Oceanologica. Sin.* 39, 33–41. doi: 10.1007/s13131-020-1543-y

Liu, F., Yuan, L., Yang, Q., Ou, S., Xie, L., and Cui, X. (2014). Hydrological Responses to the Combined Influence of Diverse Human Activities in the Pearl River Delta, China. *CATENA* 113, 41–55. doi: 10.1016/j.catena.2013.09.003

Liu, Z., Zhao, M., Sun, H., Yang, R., Chen, B., and Yang, M. (2017). "Old" Carbon Entering the South China Sea From the Carbonate-Rich Pearl River Basin: Coupled Action of Carbonate Weathering and Aquatic Photosynthesis. *Appl. Geochem.* 78, 96–104. doi: 10.1016/j.apgeochem.2016.12.014

Luo, Z., Yao, C., Li, Q., and Huang, Z. (2016). Terrestrial Water Storage Changes Over the Pearl River Basin From GRACE and Connections With Pacific Climate Variability. *Geodes. Geodynamic.* 7, 171–179. doi: 10.1016/j.geog.2016.04.008

Mantua, N. J., Hare, S. R., Zhang, Y., Wallace, J. M., and Francis, R. C. (1997). A Pacific Interdecadal Climate Oscillation With Impacts on Salmon Production**. *Bull. Am. Meteorological Soc.* 78, 1069–1080. doi: 10.1175/1520-0477(1997)078<1069:APICOW>2.0.CO;2

Meybeck, M. (1987). Global Chemical Weathering of Surficial Rocks Estimated From River Dissolved Loads. *Am. J. Sci.* 287, 401–428. doi: 10.2475/ajs.287.5.401

Mollenhauer, G., and Eglinton, T. I. (2007). Diagenetic and Sedimentological Controls on the Composition of Organic Matter Preserved in California Borderland Basin Sediments. *Limnol. Oceanog.* 52, 558–576. doi: 10.4319/lo.2007.52.2.0558

Owen, R. B., and Lee, R. (2004). Human Impacts on Organic Matter Sedimentation in a Proximal Shelf Setting, Hong Kong. *Continent. Shelf. Res.* 24, 583–602. doi: 10.1016/j.csr.2003.11.004

Paterson, G. A., and Heslop, D. (2015). New Methods for Unmixing Sediment Grain Size Data. *Geochem. Geophys. Geosyst.* 16, 4494–4506. doi: 10.1002/2015GC006070

Perdue, E. M., and Koprivnjak, J.-F. (2007). Using the C/N Ratio to Estimate Terrigenous Inputs of Organic Matter to Aquatic Environments. *Estua. Coast. Shelf. Sci.* 73, 65–72. doi: 10.1016/j.ecss.2006.12.021

Prins, M. A., Postma, G., and Weltje, G. J. (2000). Controls on Terrigenous Sediment Supply to the Arabian Sea During the Late Quaternary: The Makran Continental Slope. *Mar. Geo.* 169, 351–371. doi: 10.1016/S0025-3227(00)00087-6

Qian, C., Yu, J.-Y., and Chen, G. (2014). Decadal Summer Drought Frequency in China: The Increasing Influence of the Atlantic Multi-Decadal Oscillation. *Environ. Res. Lett.* 9, 124004. doi: 10.1088/1748-9326/9/12/124004

Qian, C., and Zhou, T. J. (2014). Multidecadal Variability of North China Aridity and Its Relationship to PDO During 1900-2010. *J. Climate* 27, 1210–1222. doi: 10.1175/JCLI-D-13-00235.1

Sánchez-García, L., de Andrés, J. R., Martín-Rubí, J. A., and Louchouarn, P. (2009). Diagenetic State and Source Characterization of Marine Sediments From the Inner Continental Shelf of the Gulf of Cádiz (SW Spain), Constrained by Terrigenous Biomarkers. *Organ. Geochem.* 40, 184–194. doi: 10.1016/j.orggeochem.2008.11.001

Seidel, M., Yager, P. L., Ward, N. D., Carpenter, E. J., Gomes, H. R., Krusche, A. V., et al. (2015). Molecular-Level Changes of Dissolved Organic Matter Along the Amazon River-To-Ocean Continuum. *Mar. Chem.* 177, 218–231. doi: 10.1016/j.marchem.2015.06.019

Smith, R. W., Bianchi, T. S., Allison, M., Savage, C., and Galy, V. (2015). High Rates of Organic Carbon Burial in Fjord Sediments Globally. *Nat. Geosci.* 8, 450–453. doi: 10.1038/ngeo2421

Smittenberg, R. H., Hopmans, E. C., Schouten, S., Hayes, J. M., Eglinton, T. I., and Damste, J. S. S. (2004). Compound-Specific Radiocarbon Dating of the Varved Holocene Sedimentary Record of Saanich Inlet, Canada. *Paleoceanography* 19 (2), 1–16. doi: 10.1029/2003PA000927

Starkloff, T., and Stolte, J. (2014). Applied Comparison of the Erosion Risk Models EROSION 3D and LISEM for a Small Catchment in Norway. *CATENA* 118, 154–167. doi: 10.1016/j.catena.2014.02.004

Sun, C., Kucharski, F., Li, J., Jin, F.-F., Kang, I.-S., and Ding, R. (2017). Western Tropical Pacific Multidecadal Variability Forced by the Atlantic Multidecadal Oscillation. *Nat. Commun.* 8 (1), 1–10. doi: 10.1038/ncomms15998

Swindles, G. T., Galloway, J. M., Macumber, A. L., Croudace, I. W., Emery, A. R., Woulds, C., et al. (2018). Sedimentary Records of Coastal Storm Surges: Evidence of the 1953 North Sea Event. *Mar. Geo.* 403, 262–270. doi: 10.1016/j.margeo.2018.06.013

Syvitski, J., Ángel, J. R., Saito, Y., Overeem, I., Vörösmarty, C. J., Wang, H., et al. (2022). Earth's Sediment Cycle During the Anthropocene. *Nat. Rev. Earth Environ.* 3, 179–196. doi: 10.1038/s43017-021-00253-w

Tao, S., Eglinton, T. I., Montluçon, D. B., McIntyre, C., and Zhao, M. (2015). Pre-Aged Soil Organic Carbon as a Major Component of the Yellow River Suspended Load: Regional Significance and Global Relevance. *Earth Planet. Sci. Lett.* 414, 77–86. doi: 10.1016/j.epsl.2015.01.004

Tareq, S. M., Tanaka, N., and Ohta, K. (2004). Biomarker Signature in Tropical Wetland: Lignin Phenol Vegetation Index (LPVI) and its Implications for Reconstructing the Paleoenvironment. *Sci. Total. Environ.* 324, 91–103. doi: 10.1016/j.scitotenv.2003.10.020

Wakeham, S. G., Canuel, E. A., Lerberg, E. J., Mason, P., Sampere, T. P., and Bianchi, T. S. (2009). Partitioning of Organic Matter in Continental Margin Sediments Among Density Fractions. *Mar. Chem.* 115, 211–225. doi: 10.1016/j.marchem.2009.08.005

Walinsky, S. E., Prahl, F. G., Mix, A. C., Finney, B. P., Jaeger, J. M., and Rosen, G. P. (2009). Distribution and Composition of Organic Matter in Surface Sediments of Coastal Southeast Alaska. *Continent. Shelf. Res.* 29, 1565–1579. doi: 10.1016/j.csr.2009.04.006

Wang, S., Zhuang, Q., Lähteenoja, O., Draper, F. C., and Cadillo-Quiroz, H. (2018). Potential Shift From a Carbon Sink to a Source in Amazonian Peatlands Under a Changing Climate. *Proc. Natl. Acad. Sci.* 115, 12407–12412. doi: 10.1073/pnas.1801317115

Wei, X., Cai, S., Ni, P., and Zhan, W. (2020). Impacts of Climate Change and Human Activities on the Water Discharge and Sediment Load of the Pearl River, Southern China. *Sci. Rep.* 10 (1), 1–11. doi: 10.1038/s41598-020-73939-8

Wei, X., Yi, W., Shen, C., Yechieli, Y., Li, N., Ding, P., et al. (2010). 14C as a Tool for Evaluating Riverine POC Sources and Erosion of the Zhujiang (Pearl River) Drainage Basin, South China. *Nucl. Instru. Methods Phys. Res. Sec. B.: Beam. Interact. Material. Atoms.* 268, 1094–1097. doi: 10.1016/j.nimb.2009.10.107

Wheatcroft, R. A., Goñ I, M. A., Hatten, J. A., Pasternack, G. B., and Warrick, J. A. (2010). The Role of Effective Discharge in the Ocean Delivery of Particulate Organic Carbon by Small, Mountainous River Systems. *Limnol. Oceanog.* 55, 161–171. doi: 10.4319/lo.2010.55.1.0161

White, H. K. (2006). Isotopic Constraints on the Sources and Associations of Organic Compounds in Marine Sediments. *Massachu. Insti. Technol* 1, 134–166. doi: 10.1575/1912/1512

Williams, E. K., Rosenheim, B. E., Allison, M., McNichol, A. P., and Xu, L. (2015). Quantification of Refractory Organic Material in Amazon Mudbanks of the French Guiana Coast. *Mar. Geo.* 363, 93–101. doi: 10.1016/j.margeo.2015.02.009

Wu, Y., Eglinton, T., Yang, L., Deng, B., Montluçon, D., and Zhang, J. (2013). Spatial Variability in the Abundance, Composition, and Age of Organic Matter in Surficial Sediments of the East China Sea. *J. Geophys. Res.: Biogeosci.* 118, 1495–1507. doi: 10.1002/2013JG002286

Wu, X. F., and Mao, J. Y. (2017). Interdecadal Variability of Early Summer Monsoon Rainfall Over South China in Association With the Pacific Decadal Oscillation. *Int. J. Climatol.* 37, 706–721. doi: 10.1002/joc.4734

Wu, Z. Y., Milliman, J. D., Zhao, D. N., Cao, Z. Y., Zhou, J. Q., and Zhou, C. Y. (2018). Geomorphologic Changes in the Lower Pearl River Delta 1850-2015, Largely Due to Human Activity. *Geomorphology* 314, 42–54. doi: 10.1016/j.geomorph.2018.05.001

Wu, W., Qu, S., Nel, W., and Ji, J. (2020). The Impact of Natural Weathering and Mining on Heavy Metal Accumulation in the Karst Areas of the Pearl River Basin, China. *Sci. Total. Environ.* 734, 139480. doi: 10.1016/j.scitotenv.2020.139480

Wu, Z. Y., Saito, Y., Zhao, D. N., Zhou, J. Q., Cao, Z. Y., Li, S. J., et al. (2016). Impact of Human Activities on Subaqueous Topographic Change in Lingding Bay of the Pearl River Estuary, China, During 1955-2013. *Sci. Rep.* 6, 37742. doi: 10.1038/srep37742

Wu, Y., Zhang, J., Liu, S. M., Zhang, Z. F., Yao, Q. Z., Hong, G. H., et al. (2007). Sources and Distribution of Carbon Within the Yangtze River System. *Estua. Coast. Shelf. Sci.* 71, 13–25. doi: 10.1016/j.ecss.2006.08.016

Yang, Q., Ma, Z., Fan, X., Yang, Z.-L., Xu, Z., and Wu, P. (2017a). Decadal Modulation of Precipitation Patterns Over Eastern China by Sea Surface Temperature Anomalies. *J. Climate* 30, 7017–7033. doi: 10.1175/JCLI-D-16-0793.1

Yang, Q., Ma, Z. G., and Xu, B. L. (2017b). Modulation of Monthly Precipitation Patterns Over East China by the Pacific Decadal Oscillation. *Climat. Change* 144, 405–417. doi: 10.1007/s10584-016-1662-9

Yang, L., Scheffran, J., Qin, H., and You, Q. (2015). Climate-Related Flood Risks and Urban Responses in the Pearl River Delta, China. *Reg. Environ. Change* 15, 379–391. doi: 10.1007/s10113-014-0651-7

Ye, Y., Bo, L., Li, S., and Hu, J. (2021). A Study on the Response of Carbon Cycle System in the Pearl River Estuary to Riverine Input Variations. *J. Mar. Syst.* 215, 103498. doi: 10.1016/j.jmarsys.2020.103498

Ye, Z., Chen, J., Gao, L., Liang, Z., Li, S., Li, R., et al. (2020). (210)Pb Dating to Investigate the Historical Variations and Identification of Different Sources of Heavy Metal Pollution in Sediments of the Pearl River Estuary, Southern China. *Mar. Pollut. Bull.* 150, 110670. doi: 10.1016/j.marpolbul.2019.110670

Yuan, X. Q., Yang, Q. S., Luo, X. X., Yu, F. L., Liu, F., Li, J. Y., et al. (2019). Distribution of Grain Size and Organic Elemental Composition of the Surficial Sediments in Lingding Bay in the Pearl River Delta, China: A Record of Recent Human Activity. *Ocean. Coast. Manage.* 178, 1–11. doi: 10.1016/j.ocecoaman.2019.104849

Zhang, Z., Leduc, G., and Sachs, J. P. (2014). El Niño Evolution During the Holocene Revealed by a Biomarker Rain Gauge in the Galápagos Islands. *Earth Planet. Sci. Lett.* 404, 420–434. doi: 10.1016/j.epsl.2014.07.013

Zhang, F., Li, S., Sun, C., Li, W., Zhao, X., Chen, Z., et al. (2022). Human Impacts Overwhelmed Hydroclimate Control of Soil Erosion in China 5,000 Years Ago. *Geophys. Res. Lett.* 49 (5), 1–10. doi: 10.1029/2021GL096983

Zhang, H., Ma, W.-C., and Wang, X.-R. (2008). Rapid Urbanization and Implications for Flood Risk Management in Hinterland of the Pearl River Delta, China: The Foshan Study. *Sensors* 8, 2223–2239. doi: 10.3390/s8042223

Zhao, B., Yao, P., Bianchi, T. S., and Yu, Z. G. (2021). Controls on Organic Carbon Burial in the Eastern China Marginal Seas: A Regional Synthesis. *Global Biogeochem. Cycle.* 35 (4), 1–27. doi: 10.1029/2020GB006608

Zheng, J., and Wang, C. (2021). Influences of Three Oceans on Record-Breaking Rainfall Over the Yangtze River Valley in June 2020. *Sci. China Earth Sci* 64, 1607–1618. doi: 10.1007/s11430-020-9758-9

Conflict of Interest: The authors declare that the research was conducted in the absence of any commercial or financial relationships that could be construed as a potential conflict of interest.

Publisher's Note: All claims expressed in this article are solely those of the authors and do not necessarily represent those of their affiliated organizations, or those of the publisher, the editors and the reviewers. Any product that may be evaluated in this article, or claim that may be made by its manufacturer, is not guaranteed or endorsed by the publisher.